High-Energy Heavy Ion Irradiation of HOPG

D. Iveković[1]*, P. Dubček[1]*, A. Gajović[1], T. Čižmar[1], B. Radatović[2], A.L. Brkić[2], M. Kralj[2], M. Karlušić[1]

1 Ruđer Bošković Institute, Bijenička Cesta 54, 10000 Zagreb, Croatia

2 Institute of Physics, Bijenička Cesta 46, 10000 Zagreb, Croatia;

Correspondence: damjan.ivekovic@irb.hr; pavo.dubcek@irb.hr

ABSTRACT

Understanding the behaviour of the graphite under extreme conditions is very important for its use in applications related to the nuclear technology. In this work, we used atomic force microscopy, scanning tunnelling microscopy, and Raman spectroscopy to study the graphite response to high-energy heavy ions irradiation. On the surface, we found ion tracks after grazing incidence ion irradiation by 23 MeV I, which makes the graphite surface susceptible to this type of irradiation. Within the bulk, no tracks have been found after normal incidence irradiation. However, we show that electronic energy loss plays a role in defect recovery, making graphite below the surface even more stable to the high-energy heavy ion irradiation.

Keywords: ion irradiation, graphite, HOPG, defects, Raman spectroscopy, AFM, STM

1. Introduction

Due to its stability at extremely high temperatures, graphite is often used in nuclear reactors as moderator and reflector of neutrons. The physical and structural changes that occur in graphite stem from the crystal lattice damage due to impact of fast neutrons and the associated recoil cascades. Therefore, understanding its radiation hardness (i.e., its stability under neutron and ion irradiation) is paramount to the safe use of graphite. Highly oriented pyrolytic graphite (HOPG) is a synthetic form of graphite of the highest quality, with a mosaic spread less than one degree. Its flat surface is suitable for analysis by scanning tunnelling microscopy (STM) and atomic force microscopy (AFM). Therefore, it has been used in many ion irradiation experiments for atomic-scale investigations of the ion impact sites [1].

Ion irradiation, nowadays widely available at ion accelerator facilities, is often used in radiation hardness studies as a tool to simulate neutron irradiation. This approach has many advantages, such as the relatively short beamtimes required to achieve high damage levels, and absence of radioactive material generation in case of irradiations with energies below Coulomb barrier [2]. Also, easily tuned ion beam parameters like ion type, energy and fluence, should be mentioned as advantages of this versatile approach [3-5]. However, the correlation between the effects of ion and neutron irradiation and resulting damage is not straightforward. In the case of

graphite, this is even more complicated by its unusual response to high-energy heavy ion irradiation.

The impact of low energy ions into the material results in generation of recoil cascades when elastic collisions with atomic nuclei result in damage formation after the atoms have come to rest in non-ideal positions (i.e. interstitial positions). At high ion energies, typically tens of MeV and above, these elastic collisions with nuclei occur less frequently , and slowing down of the incident ion within the material is almost exclusively caused by numerous inelastic collisions with electrons. In these two cases, the energy loss of the ion is called nuclear energy loss dE_n/dx and electronic energy loss dE_e/dx, respectively. The exact mechanism of the damage formation in high-energy case is still under debate. The most commonly invoked model is the thermal spike model [6-9], which envisages melting of the material along the ion trajectory because electron-phonon coupling transfers sufficient amount of energy from electron into the phonon system within a few picoseconds after the ion passage. After rapid cooling, permanent damage remains, referred to as an ion track, although in some materials recrystallization (sometimes referred to as projectile assisted prompt annealing (PAPA) [10]) makes ion tracks both smaller and more difficult to produce [11-14].

Materials containing defects (for example due to pre-irradiation by low-energy ions) are known to exhibit diverse response to high-energy heavy ion irradiation. In the case of $SrTiO_3$, damage present within the material makes it more susceptible to the ion track formation, probably due to increased electron-phonon coupling [15]. Even more surprising is that the recrystallization driven by the thermal spike can effectively erase defects in certain materials such as SiC [16,17] and Si [18]. This effect is known as swift heavy ion beam induced epitaxial crystallisation (SHIBIEC). We note that both SiC and Si are materials in which no ion tracks were found [10,19,20], unless cluster ion irradiation was used [21,22]. Clearly, recrystallization can play important role in both ion track formation and in SHIBIEC.

At the surface, recrystallization that occurs in later stages of ion track formation can be inhibited. This makes grazing incidence high-energy heavy ion irradiation a very promising tool for surface nanopatterning [23,24] because ion tracks can be formed much more easily. The unique, chain-like ion track morphology is due to localized melting when high-energy heavy ion intersects the crystal planes and encounters high electron density (which in turn transiently increases electronic energy loss) [25,26]. Previously, we have demonstrated this at high energies (~10 MeV) for various materials such as $SrTiO_3$ and TiO_2 [27], GaN [28], Al_2O_3 and MgO [29,30] and graphene [31]. At even higher energies (~100 MeV), ion tracks were also found on SiC surfaces [32].

Early transmission electron microscopy (TEM) investigations of graphite irradiated with very high-energy heavy ions (850 MeV Pb and 850 MeV U) showed no ion tracks [33]. This surprising result was explained by the mechanism of prompt recrystallization (PAPA) [10,34]. However, some material modification did take place because unirradiated samples were stable under the electron beam in TEM while irradiated samples underwent some changes (formation of carbon onions), indicating the presence of an undetected heavy ion irradiation-induced disorder at the atomic scale [33]. This result is similar to the case of silicon, another monoelemental target

where strong recrystallization is expected to hinder the ion track formation [20]. Later it was found that fullerene cluster irradiation at 20-30 MeV produced ion tracks in graphite [35]. Additionally, ion tracks were found after 850 MeV Pb irradiation at cryogenic temperature (90 K) [35] and also at the highest available ion energies (2.6 GeV U) under ambient conditions [36]. To accommodate these results within thermal spike models, non-standard model parameters had to be used [6-8].

Several STM and AFM studies found distinct topographical features formed on HOPG surfaces after high-energy heavy ion irradiation, i.e., when electronic energy loss dominates nuclear energy loss [37-46]. As discussed above, it is not unexpected to find ion tracks at the surface when ion tracks are absent in the bulk. However, somewhat puzzling was the finding that ion tracks did form roughly 5 μm in depth, as detected by means of STM, after the irradiated HOPG sample was cleaved [38]. Also, at lower ion energies, when the electronic and nuclear energy losses are of similar magnitude, surface protrusions were found after irradiation with 3 MeV Au [47] and 4.5 MeV Au [48]. In the follow-up study, different ion types (Si, Cu, As, Sr, Ag, Au) accelerated to the same energy of 3.1 MeV were used for HOPG irradiation [49]. Using STM, it was found that the probabilities of surface protrusion production (i.e. ratio of areal density of surface protrusions and applied ion fluence) scale well with nuclear energy loss, indicating that protrusions cannot be assigned to ion tracks. This is in contrast to the work of Liu et al. [42], where probabilities for production of surface protrusions scale with electronic energy loss above the threshold value of $dE_e/dx = 7.5 \pm 1.5$ keV/nm, providing strong evidence of surface ion tracks.

We note that the topographic character of the protrusions should be carefully determined. Even when operating in the constant current mode, STM images electron density of states and thus acquired information might not be topographical. Although it is not possible to achieve the same lateral resolution as in STM, AFM can provide evidence of topography when working in the tapping mode. Contact mode is less desirable because modified structure at the place of the ion impact can give rise to the increased friction between the AFM tip and the surface [50] which can lead to false height information. However, this is rather easy to establish because in that case the topography of the protrusion changes when the direction of the AFM tip is reversed [47].

Long ion tracks on HOPG surfaces were found by both STM and AFM after grazing incidence irradiations using very high-energy heavy ions [44,51]. Reported track size and the probability of their formation were larger by a factor of two when compared to tracks found after normal incidence irradiation [44]. The $\sqrt{3}\times\sqrt{3}$ R30° superstructures sometimes seen were not found around ion tracks in the high-resolution STM images. More recently, we reported well-developed ion tracks observed by AFM in tapping mode after irradiation with 23 MeV I beam at grazing incidence [18]. According to the SRIM code [52], the electronic energy loss $dE_e/dx = 6.7$ keV/nm of the ion beam used is below the reported threshold [42]. As mentioned above, this may be due to supressed recrystallization at the surface, although the “velocity effect” may also play a role [7].

Graphite irradiated with heavy ions has also been studied extensively by Raman spectroscopy (RS), both after high-energy [18,46,53-60] and low-energy irradiations [61-63]. Disorder kinetics can be monitored from the behaviour of the D band, but care must be taken in the case of low-energy heavy ion irradiation when the range of ions in graphite is less than optical skin depth (around 50 nm for green laser [46]). Fortunately, this depth is sufficiently large that

charge-state related effects of high-energy heavy ion irradiation [64], and problems related to energy dissipation from surfaces and thin films [65,66] do not affect the RS measurements. Additional information on recrystallization [59] and the transition from sp^2 to sp^3 hybridization [56] is also possible to obtain by RS.

Although the stability of HOPG with respect to heavy ion irradiation has been extensively studied, this was mostly done either in regime of very high ion energies (above 100 MeV) or low energies (below 1 MeV). Much less work has been done for high energies (~10 MeV), with a number of questions still remaining unanswered. In the present work, our aim was to investigate the response of the HOPG to heavy ion irradiation in this high energy range, when the electronic and nuclear energy losses could have comparable values. Previously, we used 23 MeV I beam to produce ion tracks on the surface by grazing ion irradiation [18], but exact value of threshold for ion track formation on the surface remained unknown. The RS analysis of HOPG irradiated with the same ion beam at normal incidence yielded damage cross section of around 1 nm^2, but the origin of this damage below the surface was also unknown. Although the experimentally reported threshold for ion track formation was found at 7.5 keV/nm for very high energy irradiations [42], the thermal spike model predicted a much lower value (around 3 keV/nm) at low energies due to the "velocity effect" [7]. Thus, it is of interest to reliably establish the threshold for ion track formation at high energies, considering possible contribution from the nuclear energy loss [67]. Finally, to the best of our knowledge, the SHIBIEC effect has not been studied in the HOPG yet.

2. Experimental details

HOPG samples (ZYA grade) were purchased from 2SPI. The lateral size of samples was 1×1 cm^2 with thickness of 0.7 mm. The ZYA grade guarantees mosaic spread of 0.4° ± 0.1°. The HOPG samples were irradiated at room temperature using 6 MV EN Tandem Van de Graaff accelerator located at the Ruđer Bošković Institute in Zagreb [68]. Various high-energy heavy ion beams were used, as shown in the Table 1. For all applied ion beams, their nuclear and electronic energy losses, along with the TRIM simulation damage prediction, were calculated using the SRIM code [52]. Ion irradiation was performed 5° off-normal incidence to avoid ion channelling, or at grazing incidence angle, which is 1.5 ± 0.5° relative to the surface (by using 4-axis goniometer at the ToF-ERDA beamline [69]).

After the ion irradiation, samples were analysed by Raman spectrometer Horiba Jobin Yvon T64000 with the shortest possible delay time. We used 532 nm solid-state laser with 7 mW power at the sample surface and 50× long working distance objective. Ex situ (i.e. under ambient conditions) STM and AFM were also applied in several modes. AFM measurements were done using NTEGRA Prima AFM (NT-MDT spectrum instruments) in the contact mode. AFM in non-contact (tapping) mode was done using JPK Nanowizard Ultra Speed AFM. The STM imaging was performed using the NanoSurf eSTM with platinum tips in the constant current mode. Acquired images from both AFM and STM measurements were processed with the Gwyddion software [68]. From the raw data (512×512 pixel), only a parabolic background was subtracted.

Ion type and energy	dE_e/dx (keV/nm)	dE_n/dx (keV/nm)	Range (μm)	TRIM (vacancies/ion)
1.8 MeV I	1.8	1.36	0.55	278.5
23 MeV I	6.72	0.271	5.55	56.1
3 MeV Cu	2.05	0.251	1.7	62.7
1 MeV O	1.33	0.021	1.12	7.4
4.5 MeV Si	3.3	0.027	2.24	8.4
18 MeV Cu	6.68	0.065	5.04	16.6
3 MeV O	2.17	0.009	2.21	2.8
12 MeV Si	4.37	0.012	4.12	3.6
12 MeV O	2.15	0.003	6.17	0.8

Table 1. Ion beams used in this work with their electronic energy losses dE_e/dx, nuclear energy losses dE_n/dx, ion ranges and estimated number of produced vacancies per ion impact (due to the nuclear energy loss) according to the SRIM code [52]. Number of TRIM vacancies was evaluated for 50 nm thick graphite target, that corresponds to the optical skin depth for green laser [46].

3. Experimental results

3.1. AFM and STM investigations of HOPG surface after grazing incidence ion irradiation

Previously, we found ion tracks on HOPG surfaces after irradiation with 23 MeV I under grazing incidence [18]. Due to the high applied fluence, it was not possible to evaluate length of the individual tracks, i.e. it was only possible to establish existence of ion tracks produced by the ion beam with electronic energy loss dE_e/dx = 6.7 keV/nm. There are several new findings that we present in Fig. 1, where images of HOPG surfaces irradiated with different ion beams in grazing incidence geometry are shown. Here, the individual tracks can be readily identified, as the fluence has been reduced.

AFM images obtained in tapping mode (Fig. 1(a)) show tracks that are rather short, less than 100 nm in length. Also, their height is small, as individual protrusions rarely exceeded 0.2 nm in height. The baseline of the ion track is also elevated and typically has a height of no more than 0.1 nm. These observations are consistent with previous findings that ion tracks on HOPG surfaces are much smaller than tracks found on surfaces of other materials [51]. Inspection of irradiated HOPG surfaces with AFM in the contact mode also reveals ion tracks, albeit much shorter ones (Fig. 1(b)). Most often, only a single protrusion can be seen, and only sometimes a faint ion tracks can be found after detailed inspection of the surface behind the protrusion in the direction of the ion beam. The observed protrusions are similar to those seen in high-resolution AFM images of irradiated CaF_2, where a large protrusion is found at the site of ion impact, followed by a typical discontinuous track consisting of several much smaller protrusions (where

high-energy heavy ion path extends below the surface) [71]. We also note that the observed differences in ion track heights are in full agreement with previous observations of ion tracks on CaF_2 surfaces [50], where measurements of the ion track height in the contact mode AFM yielded only half of the height determined by measurements in the tapping mode. Different elasticity modules of non-irradiated areas in contrast to ion tracks are likely to result in lower reported height values when contact mode is applied. This again proves that AFM measurements in the tapping mode are preferable for the investigation of ion tracks, which also provides evidence to the topographic nature of the ion tracks on the surface.

In Fig. 1(c), we show a typical image of surface ion tracks observed by STM. While measuring in the constant current mode, we track the position of the tip, which is displayed here, and which means that the image brightness represents the surface's height. The measured images exhibit discontinuous tracks consisting of protrusions aligned in the irradiation direction. Although it was not possible to achieve atomic resolution, use of this high lateral resolution technique confirmed that the ion tracks consist of individual protrusions separated from each other. The tracks found are very short, and typically consist of only a few protrusions. Similar to HOPG surfaces exposed to much higher ion energies [51], we found no additional features (like $\sqrt{3}\times\sqrt{3}$ R30° superstructures) around ion tracks. Finally, exposure of the HOPG surface to 12 MeV Si beam does not yield ion tracks, as shown in Fig. 1(d). In other words, the electronic energy loss dE_e/dx = 4.4 keV/nm was not sufficient for the formation of ion tracks. This way, we established threshold for the formation of ion tracks on the HOPG surface after grazing incidence irradiation by high-energy heavy ions at $(dE_e/dx)_{threshold}$ = 5.5 ± 1.2 keV/nm.

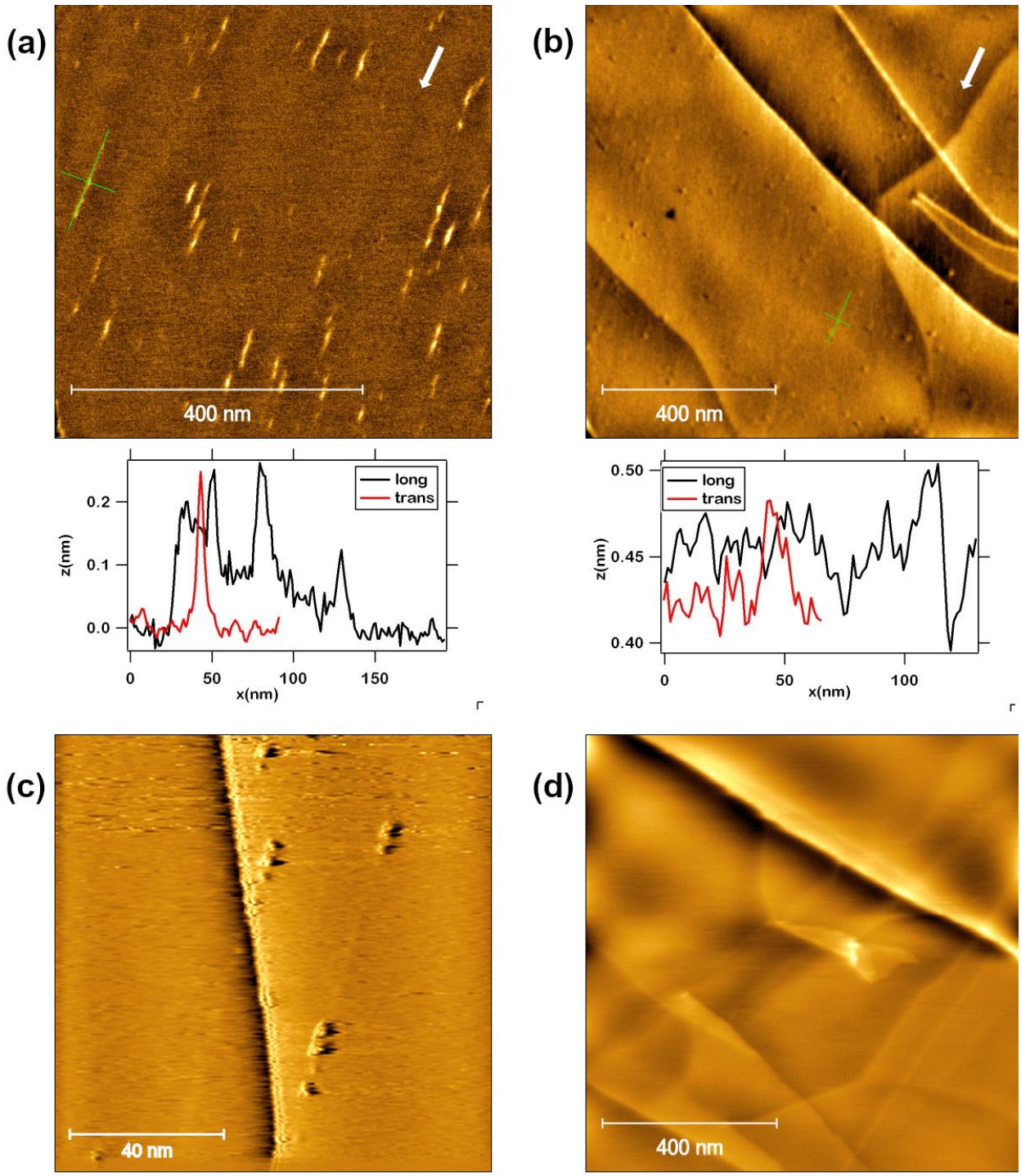

Figure 1. Ion tracks on HOPG surface observed in (a) tapping and (b) contact AFM modes. Line profiles of selected ion tracks (along the green lines in the AFM images) are also shown below as insets. Ion irradiation directions are marked by white arrows. (c) Individual ion tracks as observed by STM in constant current mode. (d) After irradiation with 12 MeV Si beam (dE_e/dx = 4.4 keV/nm) no ion tracks were found on HOPG surface by AFM in the tapping mode.

3.2. Raman spectroscopy investigation of HOPG after normal incidence ion irradiation

The disorder in the graphite structure may have more than one origin. It may be due to competing contributions of sp^2 and sp^3 phases, bond disorder, edges, sp^2 phase clustering or sp^2 ring presence. Thus, the process of amorphization is a multi-step process. In the first step, graphite is converted to nanocrystalline graphite. With further enhancement of the structural damage, low sp^3 amorphous carbon is obtained. Finally, in the last step, with further increase of structural damage, low sp^3 amorphous carbon converts to high sp^3 amorphous carbon [72,73]. Since the Raman spectrum is affected by the clustering of the sp^2 phase, the bond disorder, the presence of sp^2 rings or chains, and the sp^2/sp^3 ratio, RS is the ideal tool to study the disorder in HOPG [72,73].

Unirradiated HOPG is known to have two prominent RS bands: the so-called G band at 1580 cm^{-1} (due to stretching of sp^2 bonds) and the 2D band at ~2700 cm^{-1}. The latter is the second order of the disorder activated D band located at 1350 cm^{-1}, which can be found after ion irradiation. The D band (defect-activated breathing mode of sp^2 rings) is also often accompanied by the D' band at ~1620 cm^{-1} (an intra-valley double resonance process in the presence of defects), which is usually found only after high fluence irradiation because it is much weaker. During the growth of disorder in the first stage, the Raman spectra exhibit universal broadening of the bands, and the appearance of the D band at ~1350 cm^{-1} as well as the D' band at ~1620 cm^{-1}. Additionally, ratio of intensities of the D and G bands increases, which is considered to be directly related to the amount of disorder, both in graphene and HOPG [46,61,62].

In our previous work, we used RS to observe the accumulation of disorder in HOPG after 23 MeV I irradiation in the fluence range between 5×10^{12} - 5×10^{13} ions/cm^2 [18]. The effective cross section for disorder production $\sigma = 1nm^2$ was established using the direct ion impact model (Eq. 1). This was achieved by monitoring appearance and growth of the D-band and its relative intensity with respect to the G band. Unlike in graphene, where the Lucchese model has to be applied to correctly describe the disorder kinetics, the direct ion impact model is typically used for the analysis of disorder in HOPG because D to G band intensity ratio plateaus at high ion fluences [46]. This observed saturation essentially means that the entire sample surface is covered with ion impacts and there is no material unaffected by ion irradiation. Although the direct ion impact model is most often used to evaluate the size of ion tracks [7,74] it should be kept in mind that a good fit alone is not a proof of the existence of ion tracks. As with any other technique that indirectly quantifies ion induced damage, one must be careful in assigning the origin of the damage [75]. Therefore, our previous result is not a proof of ion tracks existence in the bulk HOPG due to 23 MeV I irradiation. To clarify this issue, and to establish threshold for ion track formation in HOPG at high ion energies, we present here RS results of HOPG irradiated with different ion beams, as specified in the Table 1, and investigate how the obtained disorder cross-sections correlate with the electronic and nuclear energy loss of the used ions. We note that electronic and nuclear energy losses are practically not changed within topmost 50 nm layer that corresponds to the optical skin depth of the green laser [46].

Since the disorder induced D band consists of two peaks (D_1 at ~1350 cm^{-1} and D_2 at ~1370 cm^{-1} [62]), we consider D to G integrated band area ratio for use in the direct ion impact model (Eq. 1):

$$\frac{A_D}{A_G} = C\left(1 - exp(-\sigma F)\right) \quad (1)$$

where A_D and A_G are the integrated areas of the D and G bands, respectively, C is the saturation value of A_D/A_G at the highest ion fluences, F is the applied ion fluence, and σ is the disorder cross-section obtained by fitting. All Raman spectra are shown in Fig. 2, and results of fitting using the procedure described above are shown in Fig. 3. For clarity, these results are also presented in the Table 2 along with the ion irradiation parameters (i.e. electronic and nuclear energy losses). Additionally, here we also present results of RS measurements on sequentially irradiated HOPG, which we did in search of possible SHIBIEC effect.

The Raman spectra shown in Fig. 2 present well-known fact that exposing HOPG to ion irradiation results in disorder induced D band that appears and grows with increasing ion fluence. The only exception is the HOPG sample irradiated by 12 MeV O, which appears to be unaffected by this particular high-energy heavy ion beam, even after exposure to the highest fluence of 3×10^{14} ions/cm^2. Other samples exhibit typical disordering behaviour, as shown in Fig. 3, which can be well-described by the direct ion impact model (Eq. 1). We note that the saturation value $C = A_D/A_G$ is similar for all ion beams used, but lower than the previously reported a value C = 1.7 [46]. In our previous work, we reported σ = 1 nm^2 for 23 MeV I irradiation, assuming this saturation value. The different value of σ = 2.5 nm^2 that we report for this ion beam in the present work is due to additional high-fluence datapoints (1×10^{14} and 2×10^{14} ions/cm^2) that establish saturation value C = 1.2 for this particular beam. These new data points and the new parameter of the fit C result in a corrected value for disorder cross-section σ = 2.5 nm^2 that we report here for the 23 MeV I beam.

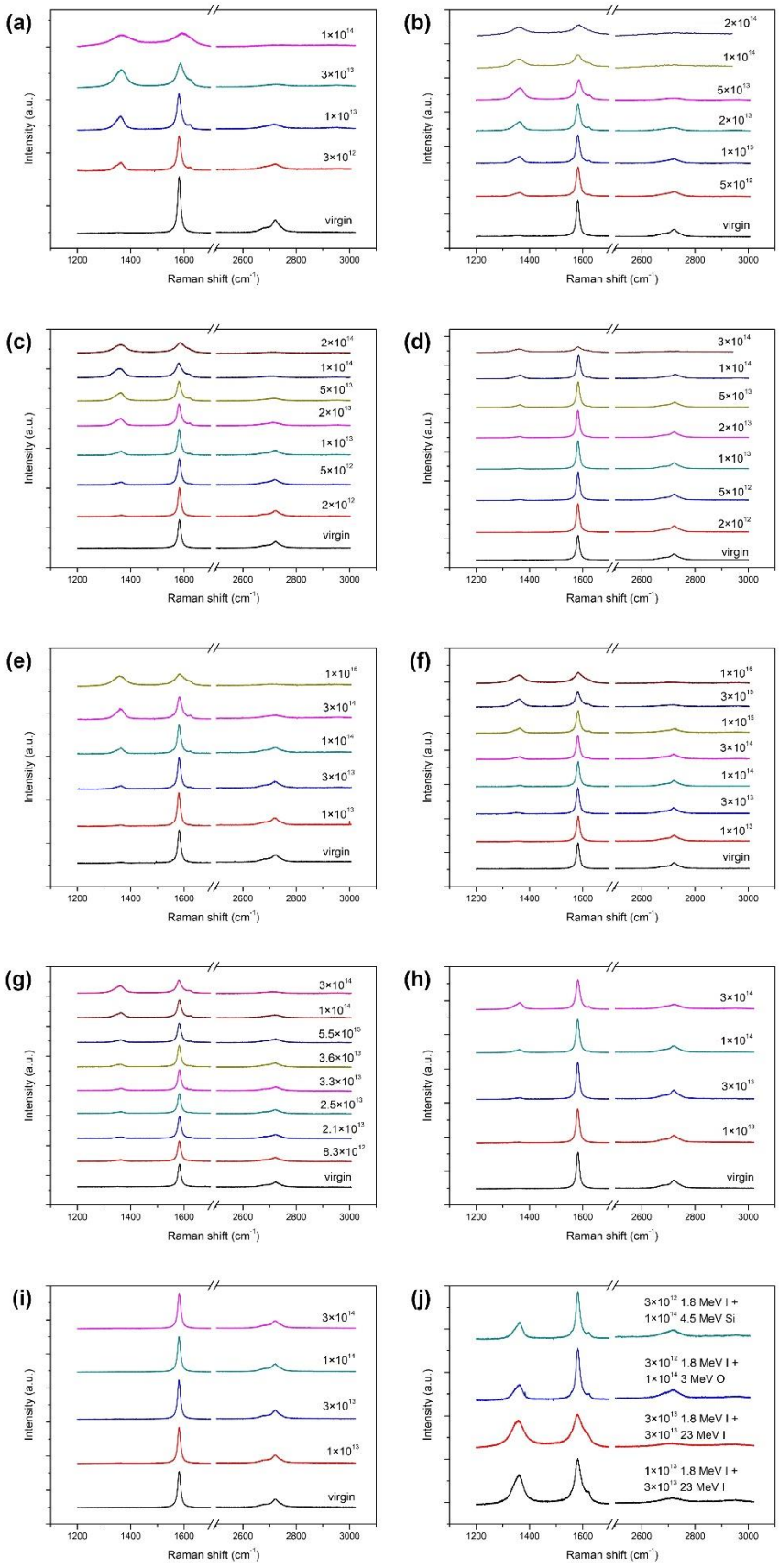
(a)
1×10^14
3×10^13
1×10^13
3×10^12
virgin
(b)
2×10^14
1×10^14
5×10^13
2×10^13
1×10^13
5×10^12
virgin
(c)
2×10^14
1×10^14
5×10^13
2×10^13
1×10^13
5×10^12
2×10^12
virgin
(d)
3×10^14
1×10^14
5×10^13
2×10^13
1×10^13
5×10^12
2×10^12
virgin
(e)
1×10^15
3×10^14
1×10^14
3×10^13
1×10^13
virgin
(f)
1×10^16
3×10^15
1×10^15
3×10^14
1×10^14
3×10^13
1×10^13
virgin
(g)
3×10^14
1×10^14
5.5×10^13
3.6×10^13
3.3×10^13
2.5×10^13
2.1×10^13
8.3×10^12
virgin
(h)
3×10^14
1×10^14
3×10^13
1×10^13
virgin
(i)
3×10^14
1×10^14
3×10^13
1×10^13
virgin
(j)
3×10^12 1.8 MeV I +
1×10^14 4.5 MeV Si
3×10^12 1.8 MeV I +
1×10^14 3 MeV O
3×10^13 1.8 MeV I +
3×10^13 23 MeV I
1×10^13 1.8 MeV I +
3×10^13 23 MeV I
Intensity (a.u.)
Raman shift (cm^-1)
1200
1400
1600
2600
2800
3000

Figure 2. Raman spectra of HOPG irradiated with (a) 1.8 MeV I, (b) 23 MeV I (data from the fluence range between 5×10^{12} - 5×10^{13} ions/cm^2 were published by us in ref. [18]), (c) 3 MeV Cu, (d) 18 MeV Cu, (e) 4.5 MeV Si, (f) 12 MeV Si, (g) 1 MeV O, (h) 3 MeV O, (i) 12 MeV O and (j) sequentially irradiated HOPG. All fluences are given in ions/cm^2.

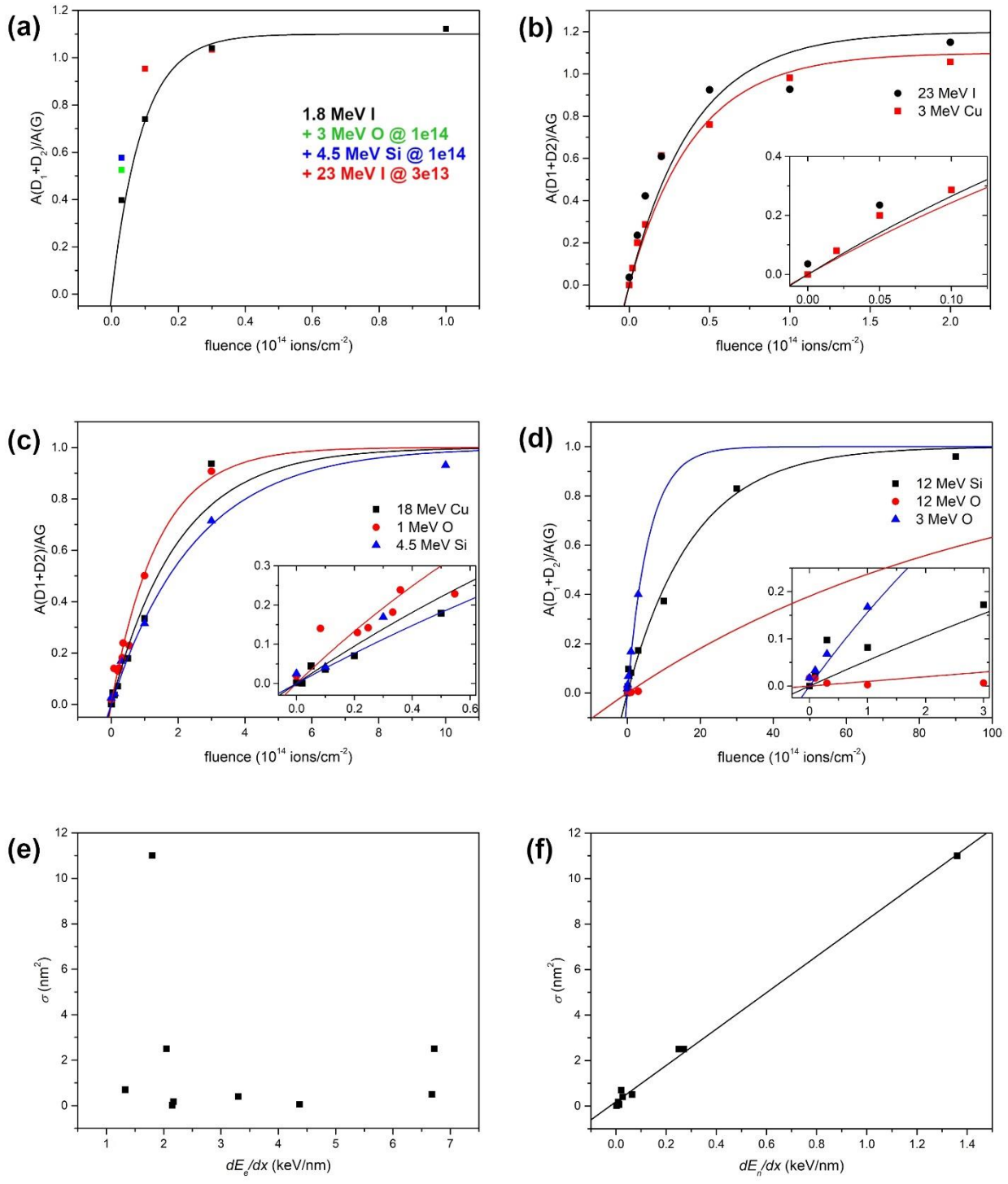

Figure 3. Results of Raman spectroscopy investigation of disorder kinetics in high-energy heavy ion irradiated HOPG. (a) Irradiations using 1.8 MeV I (black symbols) and subsequently irradiated by 3 MeV O (green, 10^{14} ions/cm^2), 4.5 MeV Si (blue, 10^{14} ions/cm^2) and 23 MeV I (red, 3×10^{13} ions/cm^2). (b) Irradiations using 23 MeV I (black) and 3 MeV Cu (red). (c) Irradiations using 18 MeV Cu (black), 1 MeV O (red), and 4.5 MeV Si (blue). (d) Irradiations using 12 MeV Si (black), 12 MeV O (red) and 3 MeV O (blue). Obtained disorder cross-sections σ (for all used ion beams) correlated with their electronic (e) and nuclear (f) energy losses.

Ion type and energy	dE_e/dx (keV/nm)	dE_n/dx (keV/nm)	σ (nm^2)	C
1.8 MeV I	1.8	1.36	11	1.1
23 MeV I	6.72	0.271	2.5	1.2
3 MeV Cu	2.05	0.251	2.5	1.1
1 MeV O	1.33	0.021	0.7	1
4.5 MeV Si	3.3	0.027	0.4	1
18 MeV Cu	6.68	0.065	0.5	1
3 MeV O	2.17	0.009	0.17	1
12 MeV Si	4.37	0.012	0.06	1
12 MeV O	2.15	0.003	0.01	1

Table 2. Results of the RS analysis of high-energy heavy ion irradiated HOPG. For each ion beam, electronic and nuclear energy losses are given according to the SRIM [52], Raman evaluated disorder cross section σ and A_D/A_G saturation value C.

As shown in Fig. 3(e,f), disorder production by the high-energy heavy ion beams we have used in this work is dominated by nuclear energy loss. There is no correlation with the electronic energy loss. As an example, we note that very small disorder cross-section $\sigma = 0.5$ nm^2 is found for the ion beam 18 MeV Cu which has the highest dE_e/dx value, like 23 MeV I. Also, for low fluences, disorder-induced D peak is negligible or even completely absent, as shown in Fig. 2(d). Therefore, we conclude that the threshold for ion track formation in the bulk HOPG is above 6.7 keV/nm. This conclusion is further supported by the finding of a linear relation between nuclear energy loss dE_n/dx and disorder cross-section σ, as shown in Fig. 3(f). The same relation holds when the nuclear energy loss is replaced by the number of vacancies produced per ion (Table 1), calculated by TRIM [52].

Since all the high-energy heavy ion beams used in the present study do not produce ion tracks within HOPG, they were suitable for investigating the possible SHIBIEC effect. For this purpose, the samples irradiated by 1.8 MeV I were additionally irradiated by 23 MeV I, 4.5 MeV

Si and 3 MeV O up to the high fluences of 3×10^{13}, 1×10^{14} and 1×10^{14} ions/cm^2, respectively. As shown in Fig. 3(a), we found only an additional disorder accumulation due to nuclear energy loss (datapoint from 1.8 MeV I irradiation up to 3×10^{13} ions/cm^2 fluence is already within the saturation region). Thus, it appears that the SHIBIEC effect is inactive in HOPG, although the material should recrystallize very effectively [10]. However, a more detailed analysis of the data presented in the Table 2 indicate electronic energy loss plays a role in the disorder production in HOPG.

4. Discussion

Raman spectroscopy results presented here agree well with already established threshold $(dE_e/dx)_{threshold}$ = 7.5 ± 1.5 keV/nm for ion track formation on the surface of HOPG after normal incidence irradiation [42]. However, theoretical prediction of $(dE_e/dx)_{threshold}$ = 3 keV/nm for ion beams having specific kinetic energy of 0.2 MeV/nucleon (like 23 MeV I, for example) underestimates experimentally established threshold $(dE_e/dx)_{threshold}$ > 6.7 keV/nm found in this work. After grazing incidence irradiation with 23 MeV I beam, short ion tracks on the HOPG surface have been found by AFM and STM. Much lower fluence used here than in our previous work [18] confirms these ion tracks are indeed features originating from the single ion impacts. Also, lower threshold for ion track formation under grazing incidence irradiation than under normal incidence, agrees well with the same observation in other materials [27-31].

Results of the sequential ion irradiation demonstrate there is no SHIBIEC effect in HOPG. Since the material is considered to exhibit exceptional recrystallisation [33,34], much like Si where SHIBIEC effect was clearly established [18], this finding is surprising. However, more detailed examination of Raman spectroscopy data provides evidence of recrystallization due to the electronic energy loss.

First, we consider data from ion irradiations using 3 MeV O, 12 MeV O and 12 MeV Si beams. As shown in the Table 2, those ion beams have comparable values of nuclear energy losses. The electronic energy loss values for these ion beams are several hundred times larger than those of nuclear energy loss. The disorder cross-sections σ obtained by RS seem to be influenced by this, in a way that disorder cross section is reduced for the ion beams with higher electronic energy losses. More precisely, σ = 0.17 nm^2 for 3 MeV O is three times larger than σ = 0.06 nm^2 for 12 MeV Si, although the nuclear energy loss is smaller for 3 MeV O (dE_n/dx = 0.009 keV/nm) than for 12 MeV Si (dE_n/dx 0.012 keV/nm). We attribute this finding to defect annealing due to the electronic energy loss which is larger for 12 MeV Si (dE_e/dx = 4.37 keV/nm) than for 3 MeV O (dE_e/dx = 2.17 keV/nm). Interestingly, the disorder annealing also appears to be affected by the nuclear energy loss as well. There is a large difference in disorder cross sections σ = 0.17 nm^2 and σ = 0.01 nm^2 for 3 MeV O and 12 MeV O beams, respectively. This can be attributed either to differences in nuclear energy losses (dE_n/dx = 0.009 keV/nm and dE_n/dx = 0.003 keV/nm, respectively) or to the "velocity effect" (since the values of electronic energy losses are practically identical, dE_e/dx = 2.17 keV/nm and dE_e/dx = 2.15 keV/nm, respectively). However, the velocity effect should cause defect annealing to be more pronounced at low velocities if thermal spikes are

responsible for the recrystallization. Since we observe the opposite (more pronounced annealing at high ion velocities), it appears that it is the amount of disorder (due to nuclear energy loss) that affects recrystallization and reduction of disorder cross-section. This could be in line with previous investigations of recrystallization effects in SiC, where similar finding was reported [17].

Next, we consider data from ion irradiations using 1 MeV O, 4.5 MeV Si and 18 MeV Cu beams. As shown in the Table 2, those ion beams have (again) comparable values of nuclear energy losses, and their electronic energy losses are 50-100× larger than corresponding nuclear energy losses. Once more, the 1 MeV O beam with the lowest value of nuclear energy loss (dE_n/dx = 0.021 keV/nm) has the highest value of the disorder cross section (σ = 0.7 nm^2). Smaller disorder cross-sections from two other beams (σ = 0.4 nm^2 for 4.5 MeV Si and σ = 0.5 nm^2 for 18 MeV Cu) can only be correlated to an increase in electronic energy losses (dE_e/dx = 3.3 keV/nm and dE_e/dx = 6.68 keV/nm, respectively) because nuclear energy losses also increase (dE_n/dx = 0.027 keV/nm and dE_n/dx = 0.065 keV/nm, respectively). Thus, 18 MeV Cu beam, which has almost three times larger nuclear energy loss than 1 MeV O, is still associated with a smaller disorder cross-section σ = 0.5 nm^2 (compared to σ = 0.7 nm^2 from 1 MeV O) due to much larger electronic energy loss.

Finally, we consider data from ion irradiations using 23 MeV I and 3 MeV Cu beams. As shown in the Table 2, those ion beams have practically identical values of nuclear energy losses, and their electronic energy losses are 25× and 8× larger than the corresponding nuclear energy losses. Obtained disorder cross-sections for those two ion beams are identical (σ = 2.5 nm^2). From this result, we conclude that the origin of the damage is primarily due to the nuclear energy loss, and that the electronic energy loss can trigger defect annealing only when it is much larger (>100×) than nuclear energy loss. Thus, in our opinion, we can exclude the possibility that the "velocity effect" plays a role in the defect recovery, which is also suggested in data set from 1 MeV O, 4.5 MeV Si and 18 MeV Cu (the velocity of these three ions does not vary much). However, the exact mechanism of damage annealing (PAPA [10] of SHIBIEC-like [17]) remains an open question.

5. Conclusion

In the present work, damage formation in HOPG due to high-energy heavy ion irradiation was studied. The AFM and STM investigation showed that the ion tracks formed after grazing incidence ion irradiation have typical topographic features (distinct protrusions along the ion trajectory), but compared to other materials, these ion tracks are very small and short. We have established a threshold for surface ion track formation at $(dE_e/dx)_{threshold}$ = 5.5 ± 1.2 keV/nm. On the other hand, using RS, we have found no evidence of the ion track formation below the HOPG surface even for the most energetic ion beam used in this work, 23 MeV I. The SHIBIEC effect was also not found after sequential ion irradiations. However, some recrystallization did occur for ion beams whose electronic energy loss was 100× greater than the nuclear energy loss. In particular, it appears that 12 MeV O beam does not produce any damage in the HOPG.

Acknowledgements

This work was supported by the Croatian Science Foundation (HRZZ pr. no. 2786). D.I. was supported in part by the ”Young Researchers’ Career Development Project – Training of Doctoral Students” of the Croatian Science Foundation funded by the European Union and the ESF. This work is partially supported by the IAEA research contract No. 23009. The authors acknowledge support from the European Regional Development Fund for the ‘Center of Excellence for Advanced Materials and Sensing Devices’ (Grant No. KK.01.1.1.01.0001).

References

[1] F. Aumayr, S. Facsko, A.S. El-Said, C. Trautmann, M. Schleberger, Single ion induced surface nanostructures: a comparison between slow highly charged and swift heavy ions, J. Phys.: Condens. Matter 23 (2011) 393001.

[2] G.S. Was, Fundamentals of Radiation Materials Science, Springer-Verlag Berlin Heidleberg (2007) 545-580.

[3] N. Galy, N. Toulhoat, N. Moncoffre, Y. Pipon, N. Bérerd, M.R. Ammard, P. Simon, D. Deldicque, P. Sainsot, Ion irradiation to simulate neutron irradiation in model graphites - Consequences for nuclear graphite, Nucl. Instr. Meth. Phys. Res. B 409 (2017) 235-240.

[4] M. Karlušić, M. Škrabić, M. Majer, M. Buljan, V. Skuratov, H.K. Jung, O. Gamulin, M. Jakšić, Infrared spectroscopy of ion tracks in amorphous SiO_2 and comparison to gamma irradiation induced changes, J. Nucl. Mater. 514 (2019) 74-83.

[5] N. Simos, P. Hurh, N. Mokhov, M. Snead, M. Topsakal, M. Palmer, S. Ghose, H. Zhong, Z. Kotsina, D.J. Sprouster, Low-temperature proton irradiation damage of isotropic nuclear grade IG-430 graphite, J. Nucl. Mater. 542 (2020) 152438.

[6] D. Schwen, E.M. Bringa, Atomistic simulations of swift ion tracks in diamond and graphite, Nucl. Instr. Meth. Phys. Res. B 256 (2007) 187-192.

[7] M. Toulemonde, W. Assmann, C. Dufour, A. Meftah, C. Trautmann, Nanometric transformation of the matter by short and intense electronic excitation: Experimental data versus inelastic thermal spike model, Nucl. Instr. Meth. Phys. Res. B 277 (2012) 28-39.

[8] M. Karlušić, M. Jakšić, Thermal spike analysis of highly charged ion tracks, Nucl. Instr. Meth. Phys. Res. B 280 (2012) 103-110.

[9] K. Nordlund, S.J. Zinkle, A.E. Sand, F. Granberg, R.S. Averback, R.E. Stoller, T. Suzudo, L. Malerba, F. Banhart, W.J. Weber, F. Willaime, S.L. Dudarev, D. Simeone, Primary radiation damage: A review of current understanding and models, J. Nucl. Mater. 512 (2018) 450-479.

[10] L.T. Chadderton, Nuclear tracks in solids: registration physics and the compound spike, Radiat. Meas. 36 (2003) 13-34.

[11] G. Szenes, Ion-induced amorphization in ceramic materials, J. Nucl. Mater. 336 (2005) 81-89.

[12] R.A. Rymzhanov, N. Medvedev, J.H. O'Connell, A. Janse van Vuuren, V.A. Skuratov, A.E. Volkov, Recrystallization as the governing mechanism of ion track formation, Sci. Rep. 9 (2019) 3837.

[13] M.C. Sequeira, J.-G. Mattei, H. Vazquez, F. Djurabekova, K. Nordlund, I. Monnet, P. Mota-Santiago, P. Kluth, C. Grygiel, S. Zhang, E. Alves, K. Lorenz, Unravelling the secrets of the resistance of GaN to strongly ionising radiation, Comm. Phys. 4 (2021) 51.

[14] H. Attariani, Latent track formation and recrystallization in swift heavy ion irradiation, Phys. Chem. Chem. Phys. 24 (2022) 24480-24486.

[15] W.J. Weber, E. Zarkadoula, O.H. Pakarinen, R. Sachan, M.F. Chisholm, P. Liu, H. Xue, K. Jin, Y. Zhang, Synergy of elastic and inelastic energy loss on ion track formation in $SrTiO_3$, Sci. Rep. 5 (2015) 7726.

[16] A. Benyagoub, A. Audren, Mechanism of the swift heavy ion induced epitaxial recrystallization in predamaged silicon carbide, J. Appl. Phys. 106 (2009) 083516.

[17] Y. Zhang, R. Sachan, O.H. Pakarinen, M.F. Chisolm, P. Liu, H. Xue, W.J. Weber, Ionization-induced annealing of pre-existing defects in silicon carbide, Nature Commun. 6 (2015) 8049.

[18] K. Tomić Luketić, M. Karlušić, A. Gajović, S. Fazinić, J.H. O'Connell, B. Pielić, B. Radatović, M. Kralj, Investigation of Ion Irradiation Effects in Silicon and Graphite Produced by 23 MeV I Beam, Materials 14 (2021) 1904.

[19] S.J. Zinkle, V.A. Skuratov, D.T. Holezer, On the conflicting roles of ionizing radiation in ceramics, Nucl. Instr. Meth. Phys. Res. B 191 (2002) 758-766.

[20] O. Osmani, I. Alzaher, T. Peters, B. Ban-d'Etat, A. Cassimi, H. Lebius, I. Monnet, N. Medvedev, B. Rethfeld, M. Schleberger, Damage in crystalline silicon by swift heavy ion irradiation, Nucl. Instr. Meth. Phys. Res. B 282 (2012) 43-47.

[21] A. Dunlop, G. Jaskierowicz, S. Della-Negra, Latent track formation in silicon irradiated by 30 MeV fullerenes, Nucl. Instr. Meth. Phys. Res. B 146 (1998) 302-308.

[22] H. Amekura, M. Toulemonde, K. Narumi, R. Li, A. Chiba, Y. Hirano, K. Yamada, S. Yamamoto, N. Ishikawa, N. Okubo, Y. Saitoh, Ion tracks in silicon formed by much lower energy deposition than the track formation threshold, Sci. Rep. 11 (2021) 185.

[23] M. Karlušić, M. Mičetić, M. Kresić, M. Jakšić, B. Šantić, I. Bogdanović-Radović, S. Bernstorff, H. Lebius, B. Ban-d'Etat, K. Žužek Rožman, J.H. O'Connell, U. Hagemann, M. Schleberger, Nanopatterning surfaces by grazing swift heavy ion irradiation, Appl. Surf. Sci. 541 (2021) 148467.

[24] K. Takahiro, K. Ozaki, K. Kawatsura, S. Nagata, S. Yamamoto, K. Narumi, H. Naramoto, Ion-induced self-organized ripple patterns on graphite and diamond surfaces, Appl. Surf. Sci. 256 (2009) 972-975.

[25] E. Akcöltekin, T. Peters, R. Meyer, A. Duvenbeck, M. Klusmann, I. Monnet, H. Lebius, M. Schleberger, Creation of multiple nanodots by single ions, Nature Nanotechn. 2 (2007) 290-294.

[26] O. Osmani, A. Duvenbeck, E. Akcöltekin, R. Meyer, H. Lebius, M. Schleberger, Calculation of electronic stopping power along glancing swift heavy ion tracks in perovskites using *ab initio* electron density data, J. Phys.: Condens. Matter 20 (2008) 315001.

[27] M. Karlušić, M. Jakšić, H. Lebius, B. Ban-d'Etat, R.A. Wilhelm, R. Heller, M. Schleberger, Swift heavy ion track formation in $SrTiO_3$ and TiO_2 under random, channeling and near-channeling conditions, J. Phys. D: Appl. Phys. 50 (2017) 205302.

[28] M. Karlušić, R. Kozubek, H. Lebius, B. Ban-d'Etat, R.A. Wilhelm, M. Buljan, Z. Siketić, F. Scholz, T. Meisch, M. Jakšić, S. Bernstorff, M. Schleberger, B. Šantić, Response of GaN to energetic ion irradiation: conditions for ion track formation, J. Phys. D: Appl. Phys. 48 (2015) 325304.

[29] M. Karlušić, R.A. Rymzhanov, J.H. O'Connell, L. Bröckers, K. Tomić Luketić, Z. Siketić, S. Fazinić, P. Dubček, M. Jakšić, G. Provatas, N. Medvedev, A.E. Volkov, M. Schleberger, Mechanisms of surface nanostructuring of Al_2O_3 and MgO by grazing incidence irradiation with swift heavy ions, Surf. Interf. 27 (2021) 101508.

[30] J. Hanžek, P. Dubček, S. Fazinić, K. Tomić Luketić, M. Karlušić, High-Energy Heavy Ion Irradiation of Al_2O_3, MgO and CaF_2, Materials 15 (2022) 2110.

[31] O. Ochedowski, O. Lehtinen, U. Keiser, A. Turchanin, B. Ban-d'Etat, H. Lebius, M. Karlušić, M. Jakšić, M. Schleberger, Nanostructuring graphene by dense electronic excitation, Nanotechnology 26 (2015) 465302.

[32] O. Ochedowski, O. Osmani, M. Schade, B.K. Bussmann, B. Ban-d'Etat, H. Lebius, M. Schleberger, Graphitic nanostripes in silicon carbide surfaces created by swift heavy ion irradiation, Nature Comm. 5 (2013) 3193.

[33] A. Dunlop, G. Jaskierowicz, L.T. Chadderton, High resolution transmission electron microscopy of GeV heavy ion irradiated graphite, Nucl. Instr. Meth. Phys. Res. B 145 (1998) 532-538.

[34] L.T. Chadderton, D. Fink, Fullerene genesis by ion beams 3: On the absence of latent tracks in GeV ion irradiated graphite, Rad. Eff. Def. Solids 152 (2000) 87-107.

[35] A. Dunlop, G. Jaskierowicz, P.M. Ossi, S. Della-Negra, Transformation of graphite into nanodiamond following extreme electronic excitations, Phys. Rev. B 76 (2007) 155403.

[36] U.A. Glassmacher, M. Lang, H. Keppler, F. Langenhorst, R. Neumann, D. Schardt, C. Trautmann, G.A. Wagner, Phase Transitions in Solids Stimulated by Simultaneous Exposure to High Pressure and Relativistic Heavy ions, Phys. Rev. Lett. 96 (2006) 195701.

[37] S. Bouffard, J. Cousty, Y. Pennec, F. Thibaudau, STM and AFM observations of latent tracks, Radiat. Eff. Def. Solids 126 (1993) 225-228.

[38] J. Liu, M.D. Hou, C.L. Liu, Z.G. Wang, Y.F. Jin, P.J. Zhai, S.L. Feng, Y. Zhang, Tracks of high energy heavy ions in HOPG studied with scanning tunneling microscopy, Nucl. Instr. Meth. Phys. Res. B 146 (1998) 356-361.

[39] L.P. Biro, J. Gyulai, K. Havancsák, Scanning probe microscopy investigation of nanometer structures produced by irradiation with 200 MeV ions, Vacuum 50 (1998) 263-272.

[40] L.P. Biro, J. Gyulai, G.I. Márk, C.S. Daróczi, Defects caused by high-energy ion beams, as measured by scanning probe methods, Micron 30 (1999) 245-254.

[41] J.P. Singh, A. Tripathi, D. Kanjilal, In situ STM studies of HOPG surface after 200 MeV Au^{+13} ion irradiation, Vacuum 57 (2000) 319-325.

[42] J. Liu, R. Neumann, C. Trautmann, C. Müller, Tracks of swift heavy ions in graphite studied by scanning tunneling microscopy, Phys. Rev. B 64 (2001) 184115.

[43] P. Nagy, B. Szabó, Zs. Szabó, K. Havancsák, L.P. Biró, J. Gyulai, A model for the hillock formation on graphite surfaces by 246 MeV Kr^{+} ions, Ultramicroscopy 86 (2001) 31-38.

[44] J. Liu, C. Trautmann, C. Müller, R. Neumann, Graphite irradiated by swift heavy ions under grazing incidence, Nucl. Instr. Meth. Phys. Res. B 193 (2002) 259-264.

[45] A. Tripathi, S.A. Khan, M. Kumar, V. Baranwal, R. Krishna, A.C. Pandey, SHI induced surface modification studies of HOPG using STM, Nucl. Instr. Meth. Phys. Res. B 244 (2006) 225-229.

[46] J. Zeng, J. Liu, H.J. Yao, P.F. Zhai, S.X. Zhang, H. Guo, P.P. Hu, J.L. Duan, D. Mo, M.D. Hou, Y.M. Sun, Comparative study of irradiation effects in graphite and graphene, Carbon 100 (2016) 16-26.

[47] H. Ogiso, W. Mizutani, S. Nakano, H. Tokumoto, K. Yamanaka, Lattice disorder and density of states change of graphite surface by single ion impact, Appl. Phys. A 66 (1998) S1155-S1158.

[48] J. Yan, Z. Li, C. Bai, W.S. Yang, Y. Wang, W. Zhao, Y. Kang, F.C. Yu, P. Zhai, Y. Tang, Scanning tunneling microscopy investigation of graphite surface damage induced by gold ion bombardment, J. Appl. Phys. 75 (1994) 1390.

[49] H. Ogiso, H. Tokumoto, S. Nakano, K. Yamanaka, Widely changing probability of surface damage creation induced by a single ion in the MeV ion energy range, J. Vac. Sci. Technol. B 16 (1998) 1914.

[50] N. Khalfaoui, M. Görlich, C. Müller, M. Schleberger, H. Lebius, Latent tracks in CaF_2 studied with atomic force microscopy in air and in vacuum, Nucl. Instr. Meth. Phys. Res. B 245 (2006) 246-249.

[51] S. Akcöltekin, E. Akcöltekin, M. Schleberger, H. Lebius, Scanning probe microscopy investigation of nanostructured surfaces induced by swift heavy ions, J. Vac. Sci. Technol. B 27 (2009) 944-947.

[52] J.F. Ziegler, M.D. Ziegler, J.P. Biersack, SRIM – the stopping and range of ions in matter (2010), Nucl. Instr. Meth. Phys. Res. B 268 (2010) 1818-1823.

[53] J. Liu, M.D. Hou, C. Trautmann, R. Neumann, C. Müller, Z.G. Wang, Q.X. Zhang, Y.M. Sun, Y.F. Jin, H.W. Liu, H.J. Gao, STM and Raman spectroscopic study of graphite irradiated by heavy ions, Nucl. Instr. Meth. Phys. Res. B 212 (2003) 303-307.

[54] J. Liu, H.J. Yao, Y.M. Sun, J.L. Duan, M.D. Hou, D. Mo, Z.G. Wang, Y.F. Jin, H. Abe, Z.C. Li, N. Sekimura, Temperature annealing of tracks induced by ion irradiation of graphite, Nucl. Instr. Meth. Phys. Res. B 245 (2006) 126-129.

[55] P.F. Zhai, J. Liu, J.L. Duan, H.L. Chang, J. Zeng, M.D. Hou, Y.M. Sun, Velocity effect of swift heavy ions in graphite studied by Raman spectroscopy, Nucl. Instr. Meth. Phys. Res. B 269 (2011) 2035-2039.

[56] J. Zeng, P.F. Zhai, J. Liu, H.J. Yao, J.L. Duan, M.D. Hou, Y.M. Sun, G.P. Li, Production of sp^3 hybridization by swift heavy ion irradiation of HOPG, Nucl. Instr. Meth. Phys. Res. B 307 (2013) 562-565.

[57] P.F. Zhai, J. Liu, J. Zeng, H.J. Yao, J.L. Duan, M.D. Hou, Y.M. Sun, R.C. Ewing, Raman spectrum study of graphite irradiated by swift heavy ions, Chin. Phys. B 23 (2014) 126105.

[58] J. Zeng, H.J. Yao, S.X. Yhang, P.F. Zhai, J.L. Duan, Y.M. Sun, G.P. Li, J. Liu, Swift heavy ions induced irradiation effects in monolayer graphene and highly oriented pyrolytic graphite, Nucl. Instr. Meth. Phys. Res. B 330 (2014) 18-23.

[59] P. Zhai, J. Liu, J. Zeng, J. Duan, L. Xu, H. Yao, H. Guo, S. Zhang, M. Hou, Y. Sun, Evidence for re-crystallization process in the irradiated graphite with heavy ions obtained by Raman spectroscopy, Carbon 101 (2016) 22-27.

[60] A. Prosvetov, G. Hamaoui, N. Horny, M. Chirtoc, F. Yang, C. Trautmann, M. Tomut, Degradation of thermal transport properties in fine-grained isotropic graphite exposed to swift heavy ion beams, Acta Mater. 184 (2020) 187-198.

[61] A. Jorio, M.M. Lucchese, F. Stavale, C.A. Achete, Raman spectroscopy study of Ar^+ bombardment in highly oriented pyrolytic graphite, Phys. Status Solidi B 246 (2009) 2689-2692.

[62] E.H.M. Ferreira, M.V.O. Moutinho, F. Stavale, M.M. Lucchese, R.B. Capaz, C.A. Achete, A. Jorio, Evolution of the Raman spectra from single-, few-, and many-layer graphene with increasing disorder, Phys. Rev. B 82 (2010) 125429.

[63] X. Wang, G. Li, L. Zhang, F. Xiong, Y. Guo, G. Zhong, J. Wang, P. Liu, Y. Shi, Y. Guo, L. Chen, Y. Chen, The surface defects of HOPG induced by low-energy Ar^+ ion irradiation, Appl. Surf. Sci. 585 (2022) 152680.

[64] K. Tomić Luketić, J. Hanžek, C.G. Mihalcea, P. Dubček, A. Gajović, Z. Siketić, M. Jakšić, C. Ghica, M. Karlušić, Charge State Effects in Swift-Heavy-Ion-Irradiated Nanomaterials, Crystals 12 (2022) 865.

[65] T. Ogawa, N. Ishikawa, T. Kai, Depth profiles of energy deposition near incident surface irradiated with swift heavy ions, Nucl. Instr. Meth. Phys. Res. B 461 (2019) 272-275.

[66] D. Iveković, P. Žugec, M. Karlušić, Energy Retention in Thin Graphite Targets after Energetic Ion Impact, Materials 14 (2021) 6289

[67] M. Toulemonde, W.J. Weber, G. Li, W. Shutthananadan, P. Kluth, T. Yang, Y. Wang, Y. Zhang, Synergy of nuclear and electronic energy losses in ion-irradiation processes: The case of vitreous silicon dioxide, Phys. Rev. B 83 (2011) 054106.

[68] M. Jakšić, I. Bogdanović Radović, M. Bogovac, V. Desnica, S. Fazinić, M. Karlušić, Z. Medunić, H. Muto, Ž. Pastuović, Z. Siketić, N. Skukan, T. Tadić, New capabilities of the Zagreb ion microbeam system, Nucl. Instr. Meth. Phys. Res. Sect. B 260 (2007) 114-118.

[69] Siketić, Z.; Bogdanović-Radović, I.; Jakšić, M.; Skukan, N. Time of flight elastic recoil detection analysis with a position sensitive detector. Rev. Sci. Instr. 2010, 81, 03305.

[70] D. Nečas, P. Klapetek, Gwyddion: An open-source software for SPM data analysis, Cent. Eur. J. Phys. 10 (2012) 181-188.

[71] E. Gruber, P. Salou, L. Bergen, M. El Kharazzi, E. Lattouf, C. Grygiel, Y. Wang, A. Benyagoub, D. Levavasseur, J. Rangama, H. Lebius, B. Ban-d'Etat, M. Schleberger, F. Aumayr, Swift heavy ion irradiation of CaF_2 – from grooves to hillocks in a single ion track, J. Phys.: Condens. Matter 28 (2016) 405001.

[72] A.C. Ferrari, J. Robertson, Interpretation of Raman spectra of disordered and amorphous carbon, Phys. Rev. B 61 (2000) 14095.

[73] A.C. Ferrari, Raman spectroscopy of graphene and graphite. Disorder, electron–phonon coupling, doping and nonadiabatic effects, Solid State Comm. 143 (2007) 47-57.

[74] O. Peña-Rodríguez, J. Manzano-Santamaría, A. Rivera, G. García, J. Olivares, F. Agulló-López, Kinetics of amorphization induced by swift heavy ions in α-quartz, J. Nucl. Mater. 430 (2012) 125-131.

[75] M. Toulemonde, S.M.M. Ramos, H. Bernas, C. Clerc, B. Canut, J. Chaumont, C. Trautmann, MeV gold irradiation induced damage in a quartz, Nucl. Instr. Meth. Phys. Res. B 178 (2001) 331-3336.